Quaternary Science Reviews 143 (2016) 120–132

Contents lists available at ScienceDirect

Quaternary Science Reviews

journal homepage: www.elsevier.com/locate/quascirev

Late Holocene vegetation and ocean variability in the Gulf of Oman

Charlotte S. Miller [a, *], Suzanne A.G. Leroy [a], Philip E.F. Collins [b], Hamid A.K. Lahijani [c]

[a] Department of Life Sciences, Brunel University London, Kingston Lane, Uxbridge, UB8 3PH, UK
[b] College of Engineering, Design and Physical Sciences, Brunel University London, Kingston Lane, Uxbridge, UB8 3PH, UK
[c] Iranian National Institute for Oceanography and Atmospheric Science, No. 3, Etemadzadeh St., Fatemi Ave., 12, Tehran, 1411813389, Iran

ARTICLE INFO

Article history:
Received 13 January 2016
Received in revised form
4 April 2016
Accepted 9 May 2016
Available online 23 May 2016

Keywords:
Pollen
Dinoflagellates
Iran
Sassanid period
Medieval Climate Anomaly
Little Ice Age
Gulf of Oman

ABSTRACT

Fossil pollen and dinocyst records in marine sequences are frequently combined to reveal the response of vegetation and ocean conditions to changes in both regional and global climate. In this study we analysed pollen and dinocysts within a clearly-laminated sediment core off the Iranian coast in the Gulf of Oman, an extremely data-poor area, to reconstruct climatic change during the Late Holocene (last 1900 years). The vegetation record from southern Iran indicates a replacement of savannah by desert formations at *c.* 910 CE, shortly after the Islamic invasion and the subsequent collapse of the Sassanid Empire. From *c.* 910 to 1145 CE, during the Medieval Climate Anomaly (MCA), the vegetation was heavily dominated by desert formations, such as Amaranthaceae, Caryophyllaceae, Asteraceae, *Centaurea* and *Calligonum*. In parallel, in the Gulf of Oman, the presence of *Impagidinium paradoxum* indicates a lack of freshwater discharge into the ocean around this time. The desert taxa of the MCA were subsequently replaced by savannah formations at *c.* 1145 CE, comprised mainly of Poaceae and Cyperaceae, corresponding to the Little Ice Age (LIA), indicating generally wetter climatic conditions. A sudden increase in *Spiniferites ramosus* (1–63%), at *c.* 1440 CE suggests an increase in the strength of the SW summer monsoon, with increased freshwater discharge into the ocean at this time. Our data indicate that over the past two millennia the NW Arabian Sea region has alternated between contrasting climatic conditions, with firstly a humid phase equivalent to the cultural period of the Sassanid Empire, a significantly drier climate during the MCA and a relatively wetter climate during the LIA. The mechanisms resulting in dry conditions during the MCA in the Middle East associated with the northward shift of the ITCZ and the intensification of the Indian summer monsoon may be similar to those causing the dry conditions which dominated the Early Holocene in the Near East. Our palaeoenvironmental proxy data support current observations that a globally anthropogenically-induced warmer climate is likely to lead to increased drought severity in the Middle East, putting additional stress on governments already struggling with poverty and social tensions.

1. Introduction

Observations show that globally-averaged combined land and ocean surface temperatures have risen by 0.85 °C over the last century (1880–2012 CE; Hartmann et al., 2013). These global rises in temperature have impacted natural and human systems on all continents (Hartmann et al., 2013). In extreme cases many regions have seen significant changes in precipitation, which led to increased floods, droughts and heat waves, profoundly altering ecosystem dynamics as well as disrupting food production and water supply (Min et al., 2011; Dai, 2013). Although model-simulated soil moisture, drought indices and precipitation-evaporation models suggest an increase in the risk of drought during the 21st century (Rind et al., 1990; Wang, 2005; Seager et al., 2007; Burke and Brown, 2008; Sheffield and Wood, 2008; Dai, 2013), large differences still occur between the globally observed and simulated drought patterns (Dai, 2013). Environmental reconstruction of regional climates over periods of known past globally-warm climates can help: i) to assess the environmental impact of globally-warm climates on terrestrial and marine ecosystems, and ii) to evaluate the capabilities and the limitations of global climate models, further increasing our confidence regarding future model predictions.

* Corresponding author. Department of Geosciences, University of Oslo, PO Box 1047, Blindern, Oslo, 0316, Norway.
E-mail address: c.s.miller@geo.uio.no (C.S. Miller).

http://dx.doi.org/10.1016/j.quascirev.2016.05.010

The warmest period of the last 2000 years, prior to the 20th century, was likely between 1000–1270 CE, the 'Medieval Climate Anomaly' (MCA; Lamb, 1977; IPCC, 2013). Numerous studies have attempted to produce environmental reconstructions over the MCA, in order to define medieval warmth, concluding that the warmth was heterogeneous in terms of its precise timing and regional expression (Jones and Mann, 2004; Graham et al., 2011; Guiot, 2012; IPCC, 2013). Continental-scale surface temperature reconstructions show, with high confidence, that in some regions, multi-decadal periods during the MCA were as warm as during the late 20th century (IPCC, 2013). Recent studies indicate that medieval warmth was indeed a global phenomenon, felt as far away as the western Pacific (Rosenthal et al., 2013). Nevertheless, with only a few high-resolution records from the tropics and the southern hemisphere, it is still problematic to make accurate estimates of global temperatures over the MCA (Bradley et al., 2003). To reduce the uncertainty and to make meaningful estimates of global medieval climatic conditions and the associated ecosystem response, more palaeoclimatic series must be produced with wider geographic coverage (IPCC, 2007).

Over the last century much of the Middle East, Iran in particular, has been experiencing severe drought. In the year 2000, the United Nations estimated that drought cost Iran over 3.5 billion dollars (Abbaspour et al., 2009; Moradi et al., 2011). In many parts of Iran, water supply is solely dependent on groundwater (Abbaspour et al., 2009). Over the past two decades overexploitation of water resources has caused a drawdown in the water table in most of the 600 aquifers in Iran (Motagh et al., 2008). Additionally, models predict a future decrease in groundwater recharge in already water-scarce regions in the south and east of the country (Abbaspour et al., 2009). It is now becoming increasingly important to focus efforts on understanding the factors controlling precipitation variability in the region. It is uncertain whether recent multi-decadal drought is anomalous in the context of Late Holocene climate variability, because long instrumental records and palaeoclimatic reconstructions in the Middle East are lacking (Molavi-Arabshahi et al., 2015). Analysing palaeoclimatic reconstructions across periods of globally-warm temperatures in the Middle East will provide insight into how ecosystems may respond in the face of anthropogenic global warming.

By analysing both pollen grains and organic-walled dinoflagellate cysts (dinocysts) from sediment core OS73, off the southern Iranian coast, the aims of this investigation are therefore to: i) reconstruct the vegetation history in the region of southern Iran, ii) reconstruct marine conditions in the Gulf of Oman, both throughout the last 1900 years with focus on the MCA, and iii) suggest the likely environmental response of the region to future climate change.

2. Settings

2.1. Prevailing climate

The climate of Iran is defined as subtropical with hot and dry weather in the summer, with the primary cause of annual rainfall variability been the changing position of synoptic systems and year-to-year variation of the frequency of cyclones passing through the region (Modarres and Rodrigues, 2007). A large high pressure system is present throughout the year over the majority of south-west Asia (Snead, 1968). Over half of the country receives less than 200 mm yr^{-1} of precipitation with over 75% receiving less than 300 mm yr^{-1} (Dinpashoh et al., 2004). The country's average rainfall is 260 mm yr^{-1}, with the coefficient of variation varying from 18% in the north to 75% in southeast (Dinpashoh et al., 2004). The core OS73 site, in the Gulf of Oman, is positioned just above the northern extent of the ITCZ, placing it in the zone of climatic transition between the Indian summer monsoon and the Mediterranean depressionary system (Meher-Homji, 1971, Fig. 1). Rainfall in the Chabahar region occurs between October and June with no rainfall during the summer months. The hot, dry summers along the southern Makran coasts are almost void of rain due to 'capping' by subtropical high pressure. The annual temperature dataset is incomplete, but the available data indicate average temperatures of 33.5 °C (New et al., 2000).

2.2. Modern vegetation

Five vegetation biomes have been recognised in the Middle East by Olson et al. (2001): i) deserts and xeric shrublands, ii) temperate broadleaf and mixed forests, iii) montane grasslands and shrublands, iv) temperate grasslands, savannahs and shrublands, and v) flooded grasslands and savannahs. The most extensive biomes in the Middle East are deserts and xeric shrublands, with montane grasslands and shrublands and flooded grasslands and savannahs limited to small areas at high altitude or within the Tigris-Euphrates alluvial salt marshes, respectively (Olson et al., 2001). These five vegetation biomes have been further subdivided into twelve ecoregions that have characteristic vegetation associations which are, in turn, related to the prevailing climate conditions (Fig. 1; Olson et al., 2001).

The Iranian continent immediately north of core site OS73 lies

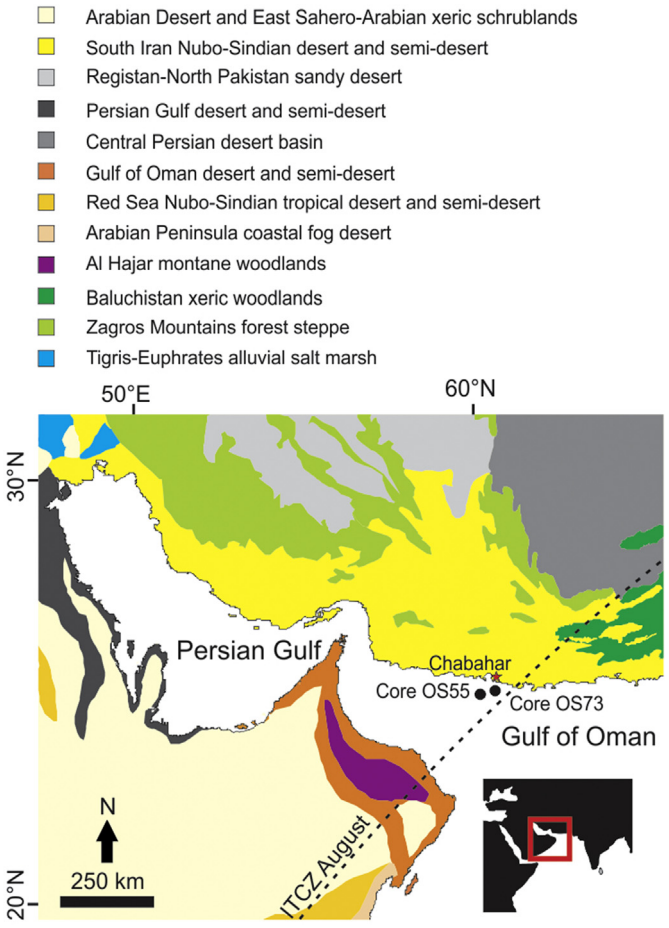

Fig. 1. Map of the modern vegetation ecoregions of NE Arabian Peninsula and S Iran (Olson et al., 2001) with the location of core site OS73 (this study), OS55 (Miller et al., 2013) and the summer ITCZ.

within the deserts and xeric shrubland biome and is within the South Iran Nubo-Sindian desert and semi-desert ecoregion (Fig. 1; Olson et al., 2001). Key formations in the region include, Acacieta flavae iranica and Nubo-Sindian classes (*e.g. Euphorieta laricae*), as well as pockets of littoral saltland vegetation such as *Salicornietea europaeae*, *Halocnemetea strobilacei* and *Suadetea deserta* (Zohary, 1973). Mangroves extend E-W along the Makran coastline, occurring in restricted pockets, the majority of which are *Avicennia marina*, a species well adapted to high salinity and dry environments (Spalding et al., 1997). *Rhizophora mucronata*, *Ceriops tagal* and *Bruguiera conjugata* occur closer to the mouth of the Indus River, and are adapted to more brackish waters and wetter environments. Two species of mangrove (*Avicenna marina* and *Rhizophora mucronata*) have been recorded as far west as the Strait of Hormuz, 137 km east of Bandar Abbas (Danne-kar, 2005). Presently, *Avicennia* is planted in the region around Chabahar (Fig. 1), however, the extent of its natural presence in the region is not known (M. Akhani, pers. comm. 2015; Milani et al., 2013).

2.3. Modern ocean conditions

The seasonal migration of the intertropical convergence zone (ITCZ) and the associated semi-annual reversal of wind patterns, the SW monsoon in the boreal summer and the NE monsoon in the boreal winter are key components of the oceanography in the Gulf of Oman. In the boreal summer the ITCZ moves to its northernmost position and differential heating of continental and oceanic regions leads to the development of areas of low atmospheric surface pressures over Iran, Pakistan, India and Oman, as well as relatively high surface pressures over the southerly cooler Indian Ocean (Zonneveld and Jurkschat, 1999). This results in the development of a strong low-level jet stream (Findlater Jet; Smith et al., 1991) and of the Somali Boundary Current (Schott et al., 1996). The boundary current causes the upwelling of cool, nutrient rich waters along the Somali and Arabian coasts, enhancing levels of primary productivity to <2.5 g C m^{-2} day^{-1} in near-coastal waters (Brock et al., 1991). Chlorophyll *a* concentrations within the surface waters of the Gulf of Oman are highest during the SW monsoon (Qasim, 1982). In the boreal winter the ITCZ moves southwards and the Eurasian continent cools, consequently a high-pressure region develops on the seasonally snow-covered Tibetan plateau and northeast winds persist over the Gulf of Oman, cooling surface water temperatures (Wyrtki, 1973). The cool winds from the northeast induce increased mixing and cooling in the Gulf of Oman and on the Pakistan shelf, which results in exceptionally high primary production in these regions (Qasim, 1982; Smith et al., 1991; Zonneveld and Jurkschat, 1999).

As a consequence of the semi-arid to arid climatic regime around Chabahar (Fig. 1), the southern Iranian coastline is made up of ephemeral streams and rivers, flowing only in times of torrential downpour during the monsoon months. The intense 'baking' of sediments during the dry months influences greatly the porosity and permeability of the channel beds and in many ephemeral channels a layer of fines is found in the upper few centimetres of riverbed sediments reducing the hydraulic conductivity of the channel bed (El-Hames and Richards, 1998). The lack of fluvial input into the northern Arabian Sea indicates that most of the sediment deposited in the coastal regions is of aeolian origin, or initially of aeolian origin and consequently redeposited by the infrequent flash floods.

2.4. Palaeoenvironmental studies in the region

In extremely arid environments continuous records of past environmental change are exceptionally rare with most records often discontinuous. Consequently, the history of vegetation and climate change in Iran is poorly understood, especially in the south (Djamali et al., 2008). The number of late-glacial and Holocene pollen records is gradually increasing, but these are mainly located in the Caspian Sea region and in the Zagros Mountains (Van Zeist and Bottema, 1977; Bottema, 1986; Leroy et al., 2007, 2011, 2013a, 2013b, 2014; Sharifi et al., 2015). Long terrestrial pollen records from Iran are exceptionally rare, e.g. Lake Zeribar, W Iran spanning the last *c.* 42,000 cal yr BP (Van Zeist and Bottema, 1977), and Lake Urmia, NW Iran covering the last *c.* 200,000 years (Djamali et al., 2008). The Makran coastline is tectonically active and prone to cyclones and flash floods, and previous studies have examined marine sediment cores in the Gulf of Oman to identify palaeoevents (Miller et al., 2013). Most long, continuous, palaeoenvironmental records available from the region come from marine sedimentary successions (Ivory and Lézine, 2009), but often lack the sampling resolution needed to reconstruct short-lived environmental perturbations (e.g. Ansari and Vink, 2007; Lézine, 2009).

Further afield, oxygen isotopes from speleothems in Oman (Fleitmann et al., 2003) and pollen records from palaeolakes in Yemen (Lézine et al., 2007) and in Oman (Parker et al., 2004) have yielded more high-resolution records indicating fluctuations in the strength of the Indian summer monsoon during the Holocene. On longer timescales, multi-proxy records from the western Arabian Sea indicate that during glacial maxima (*c.* 18,000 yr ago) monsoon circulation was weaker and stronger during the interglacial (*c.* 9000 yr ago; Prell and Campo, 1986). Furthermore, with increased monsoonal wind strength, biological productivity is thought to have reached maxima during the early Holocene when sea surface temperatures (SST) also increased (Overpeck et al., 1996). In NW Iran, sediment cores from Lake Almalou and the Caspian Sea indicate low water levels during the MCA (Omrani et al., 2007), and higher water levels during the LIA, possibly linked to periods of minimum solar insolation, through lower evaporation or even higher annual precipitation (Kroonenberg et al., 2007; Djamali et al., 2009; Leroy et al., 2011; Naderi Beni et al., 2013a,b; Haghani et al., 2015).

3. Materials and methods

3.1. Sediment recovery and chronological framework

A 141 cm-long sedimentary succession (core OS73) was retrieved in 2006 by the Iranian National Institute for Oceanography and Atmospheric Sciences at 25°08.20′N, 60°49.95′E (Fig. 1), at a water depth of 100 m. Thirteen ^{210}Pb measurements and three AMS radiocarbon ages (see Supplementary Table 1) were established from core OS73 (Fig. 2). The ^{210}Pb chronology was constructed using an Ortec Alpha Spectrometer housed at Brunel University London (UK). Detection limits depend on radionuclide alpha energy, count time and sample mass, but were typically ~12 Bq kg. Radiocarbon ages were obtained from three gastropod shells picked at 141, 120.5, 86.5 cm depth by Beta Analytic and the ^{14}CHRONO Centre (Queen's University Belfast, UK). The ^{14}C ages were calibrated using the calibration database MARINE13 (Stuiver and Reimer, 2005). The age-model was produced using the non-bayesian age model software CLAM, by linear interpolation between dated levels (Fig. 2).

3.2. Sediment description

The volume of magnetic susceptibility (MS) was measured using a Bartington MS2 magnetic susceptibly system equipped with a MS2C whole-core logging sensor, prior to grain-size (GS)

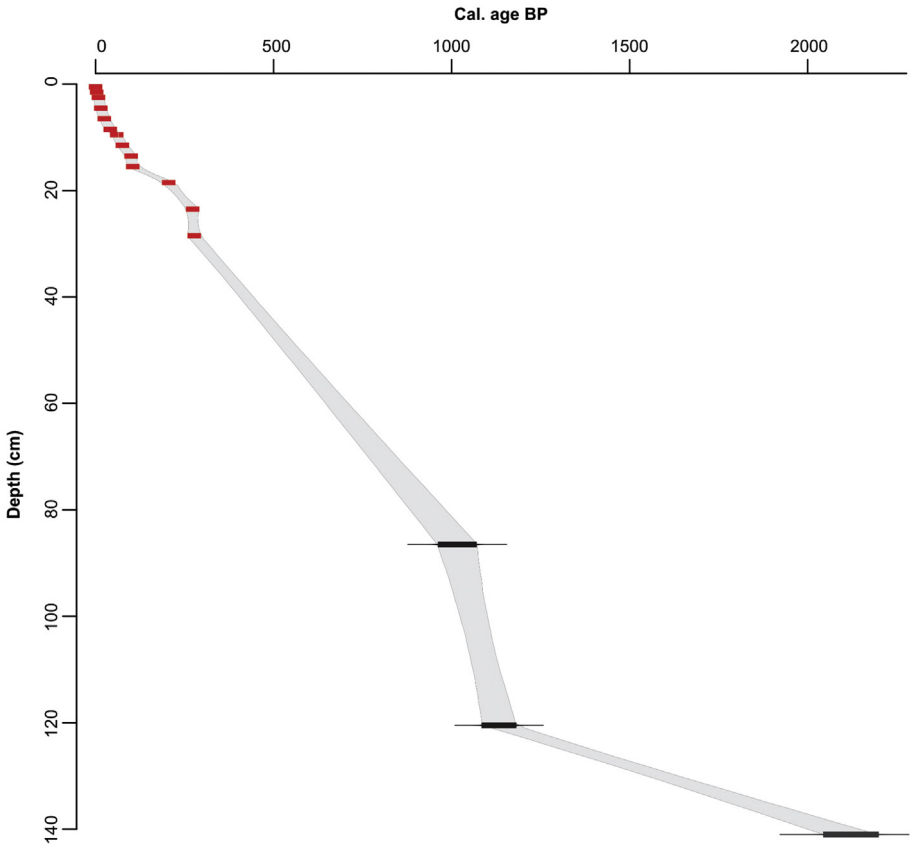

Fig. 2. Relationship between sediment depth and age for core OS73, produced by CLAM software using linear interpolation (Blaauw, 2010). Red boxes are 95% highest posterior density (hpd) ranges of ^{210}Pb ages, and black boxes are 95% hpd ranges of calibrated radiocarbon ages. Grey envelopes show 95% confidence intervals. (For interpretation of the references to colour in this figure legend, the reader is referred to the web version of this article.)

determination, using a Cilas 1064 laser particle size analyser (133 samples, including the bioclastic component). GS data were reduced using Size Expert with graphed parameters determined offline using the Folk and Ward (1957) φ method in GRADISTAT (Blott and Pye, 2001).

3.3. Fossil pollen and dinoflagellate cyst analyses

To reconstruct past vegetation and marine conditions in the region of southern Iran, we analysed 33 samples at a decadal to centennial temporal resolution for fossil pollen and dinocysts. The samples were prepared using the following procedure: sodium pyrophosphate, 10% HCl, concentrated HCl, 60% HF, concentrated HCl and, finally sieving at 125 and 10 μm. Acetolysis was not used as it destroys dinocysts. Unstained pollen and dinocysts were counted under a light microscope at a routine magnification of 400 ×, and of 1000 × for special identifications. Concentrations were calculated with reference to known abundances of the exotic marker *Lycopodium* (Stockmarr, 1972). Although concentrations were low in all samples (average = 2276 grains cm^{-3}), pollen sums were >300 terrestrial pollen grains. The identification of pollen grains was achieved using the pollen reference collections held at The Open University and at Brunel University London, as well as pollen reference guides (Faegri and Iversen, 1989; Reille, 1995; Lézine, 2005; Gosling et al., 2013). At least 200 dinocysts were counted per sample, with an average count size of 376. Dinocysts were identified using Rochon et al. (1999) and Zonneveld et al. (1997). Fossil pollen and dinocyst diagrams were then plotted to show the detailed assemblages using C2 software (Juggins, 2005). Statistical comparison of fossil pollen and dinocyst assemblages was achieved using the detrended correspondence analysis (DCA) function in Psimpoll (Bennett, 2003). DCA was performed on all pollen (and dinocyst) database(s) and included all taxa reaching an abundance of >1% of the pollen (dinocyst) sum in at least one sample (14 pollen (26 dinocyst) taxa). To identify periods of vegetation dominance by grassland (*vs* desert) taxa the diagram was 'zoned', and all samples were classified where grass (Poaceae) pollen comprised <10% of the pollen sum in three consecutive samples, as desert. The changing ratio between Amaranthaceae pollen (characteristic desert taxa) and Poaceae pollen (characteristic savannah taxa) is important and can inform regarding the temporal and spatial migration of vegetation ecoregions (Hooghiemstra et al., 2006). Nevertheless, it is important to note that a lack of detailed modern vegetation studies in the Middle East leads to difficulties in interpreting the fossil pollen record, which in this study, has been performed with caution. To identify periods of dominance by fully marine *vs* upwelling associated dinoflagellate taxa, we zoned the diagram by classifying all samples where *Impagidinium paradoxum* comprised >3% of total dinocyst sum as fully marine. *I.paradoxum* was chosen as the discriminator between marine and upwelling conditions because of its abundance within the OS73 dinoflagellate cyst record and as its distribution is strictly limited to regions characterised by fully marine conditions, with salinity ranging between 33 and 36.4 psu (Rochon et al., 1999). The ratio between pollen and dinocysts (PD) was calculated by dividing the pollen sum by the dinocyst sum, to enable the quantification of organic flux, i.e. terrestrial *vs* marine input (McCarthy and Mudie, 1998; de Vernal, 2009).

4. Results

4.1. Chronology

The age model indicates three different rates of sedimentation through the core, with the entire 141 cm long sediment core spanning the last *c.* 2120 years (Fig. 2). The oldest section of core OS73 (141–120.5 cm) has the slowest sedimentation rate of 0.21 mm/yr. The middle section of the core (120.5–86.5 cm) has the fastest sedimentation rate of 2.74 mm/yr. From 86.5 cm to core top the sedimentation rate is 0.86 mm/yr.

4.2. Sediment description and magnetic susceptibility

Grain-size (GS) determination indicates mostly homogenous silt-sized sedimentation (*c.* 89% silt, 10% clay, 0.15% sand) from the base until 17.5 cm (Fig. 3), with one sample at 89.5 cm comprising almost 100% silt. A shift in sedimentation occurs at 17.5 cm until core top, beginning with a 2 cm thick bed (17.5–15.5 cm) comprised of fine material (*c.* 65% silt, 34% clay, 0% sand). From 15.5 cm until core top, the GS analysis indicates fine silt-sized sedimentation (*c.* 77% silt, 22% clay, 0% sand). Overall, a slight increase in clay percentages occurs between 110.5 and 49.5 cm (Fig. 3). Sorting, skewness and kurtosis complement the variations in GS (Fig. 3). For example, an increase in mean GS (from 8 to 10 μm) at 76.5 cm corresponds to an increase in sorting (from 1.72 to 1.8 φ). However the relationship between mean GS and sorting does not hold true in all samples, where an increase in mean GS from 9 to 11 μm at 89.5 cm corresponds to a large decrease in the degree of sorting from 1.67 to 0.94 φ. According to Folk and Ward (1957), the whole core is poorly sorted, with the exception of a sample at 89.5 cm, which is very moderately sorted. The majority of core OS73 is fine or very-finely skewed (Fig. 3). Kurtosis values are exceptionally stable from the base of the core until 15.5 cm (except the sample at 89.5 cm), arranged around a mean of 0.81 K_G. At 15.5 cm kurtosis values drop and average at 0.71 K_G until core top. Kurtosis peaks to 1.26 K_G at 89.5 cm. The volume of MS fluctuates around a mean of 5.5 SI and does not precisely correlate with changes in GS (Fig. 3). Nevertheless MS does increase gradually up-core, presumably relating to the gradual decrease in GS (Fig. 3). The highest peak of

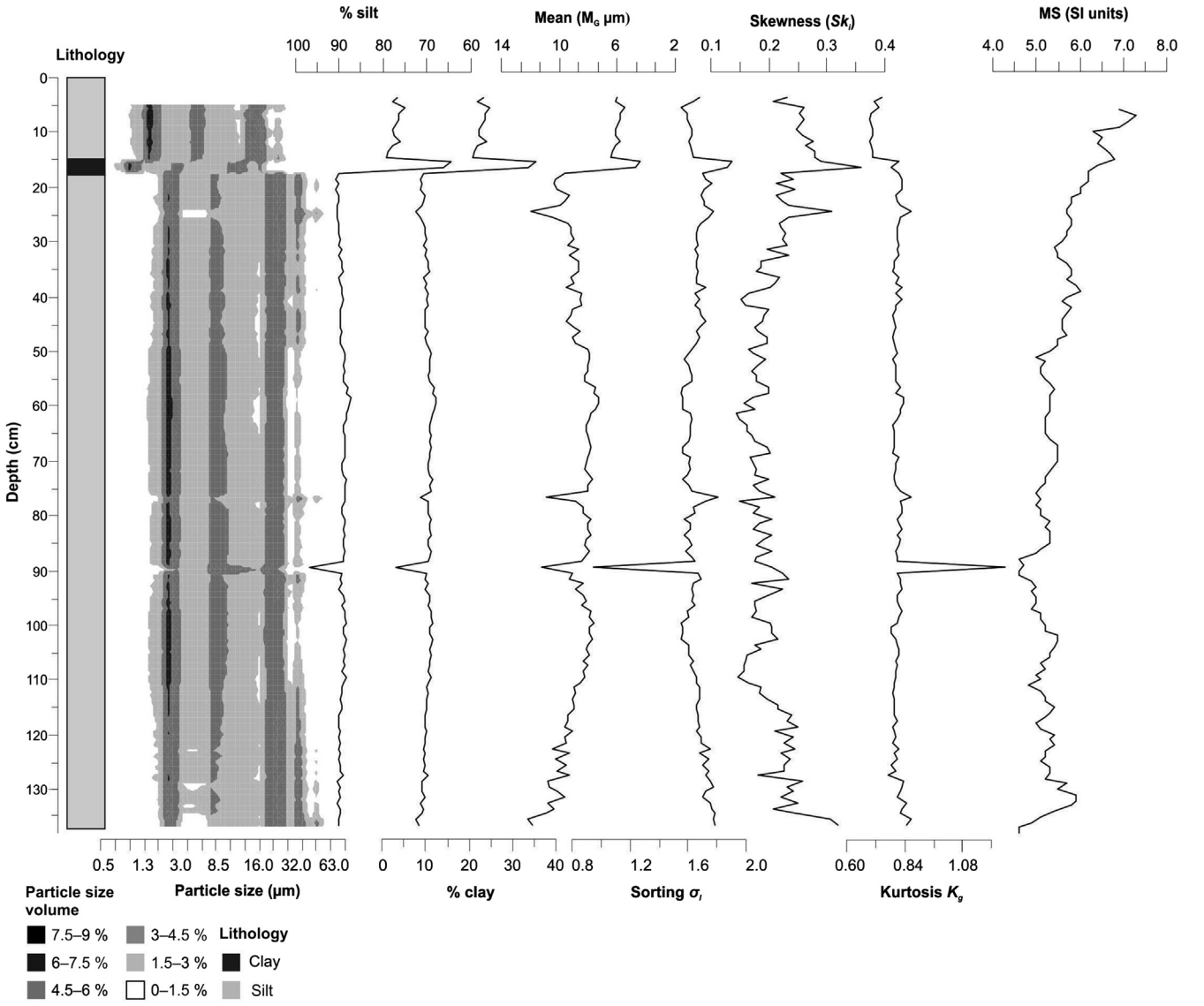

Fig. 3. Sedimentological log for core OS73 with statistical grain-size parameters and magnetic susceptibility. High-resolution particle size distribution (μm) is shown as a surface plot by volume %. Statistical grain-size analysis was performed using GRADISTAT (Blott and Pye, 2001) after Folk and Ward (1957). MS: magnetic susceptibility.

MS is at 7 cm where values reach 7.3 SI. At 138 cm, MS reaches its minimum at 4.6 SI.

4.3. Pollen analysis

In total 17 pollen taxa were identified (Fig. 4a and Supplementary Material Fig. 1). Average pollen concentrations were low at *c.* 2276 grains cm^{-3}. Taxa are plotted as percentage abundances, which were calculated as a percentage of the sum of pollen counted (excluding varia, aquatic pollen and spores). Generally pollen assemblages are dominated by *Artemisia*, Amaranthaceae and Poaceae, with sub-division of the succession into three pollen zones (Pz).

4.3.1. Pz1, 135.5–110.5 cm (c. 1857–1099 cal yr BP), 4 samples

Pz1 is dominated by relatively stable abundances of *Artemisia* and Amaranthaceae averaging at 22 and 38% respectively. Pz1 has low but stable abundances of *Calligonum*, *Pinus*, *Plantago* and Apiaceae throughout. The relative abundances of Poaceae and Cyperaceae are relatively high throughout Pz1 averaging at 15 and 3%. Percentages of Caryophyllaceae, Asteraceae and *Centaurea* are low within Pz1.

4.3.2. Pz2, 110.5–74.5 cm (c. 1099–863 cal yr BP), 6 samples

Pz2 is characterised by a gradual increase (to a maximum of 49% at 74.5 cm) in Amaranthaceae. Additionally *Artemisia* displays an increase reaching 36% at 91.5 cm. Percentages of Caryophyllaceae, Asteraceae, *Betula* and *Centaurea* increase averaging at 1, 1.8, 6.1 and 2.2%, respectively. Poaceae abundances clearly decrease from 13.9 to 4.6% at 110.5 cm and remain low through Pz2, averaging at 3.6%.

4.3.3. Pz3, 74.5–1.5 cm, (863–3 cal yr BP), 23 samples

Pz3 is characterised by first a decrease in Amaranthaceae from 49% (at 74.5 cm, within Pz2) to minimal values of 20% at 40.5 cm, and then an increase again towards the end of the zone. Percentages of *Artemisia* show a high degree of variability throughout Pz3. Caryophyllaceae, Asteraceae and *Centaurea* percentages decrease in Pz3. The relative abundance of Poaceae and Cyperaceae are high throughout Pz3 averaging at 13 and 6%. Poaceae reaches their maximal diagram abundance (25%) at 11.5 cm.

4.3.4. Fossil pollen ordination

DCA was applied to the pollen assemblages to identify trends and aid in interpretation (Fig. 5). Pollen taxon scores were grouped on the DCA according to their modern ecological affinities (Olson et al., 2001). Taxon scores of Poaceae and Cyperaceae plot negative on DCA axis 1 (Fig. 5a). Taxon scores of all other taxa including Amaranthaceae, Asteraceae and *Calligonum* plot positive on axis 1 (Fig. 5a). Generally, sample scores from Pz1 and Pz3 plot more negatively on DCA axis 1, whilst sample scores from Pz2 plot more positively on axis 1 (Fig. 5b).

4.4. Dinoflagellate cyst analysis

In total 26 dinoflagellate cyst taxa were identified (Fig. 4b). Average dinoflagellate cyst concentrations were low at *c.* 3145 grains cm^{-3}. Taxa are plotted as percentage abundances, which were calculated as a percentage of the sum of dinoflagellate cysts counted. Generally the dinoflagellate cyst assemblage is dominated by *Bitectatodinium spongium*, *Spiniferites ramosus*, *Brigantedinium* and *I. paradoxum*, with sub-division of the succession into three dinoflagellate cyst zones (Dz).

4.4.1. Dz1, 135.5–95.5 cm (1857–1047 cal yr BP), 7 samples

Except for *Brigantedinium*, this zone is characterised by relatively stable dinoflagellate cyst percentages within individual species (Fig. 4b). Additionally, small fluctuations are observed with *B. spongium* increasing from 50 to 55% between 135.5 and 110 cm, constituting the majority of the dinocyst population. *Brigantedinium* reaches *c.* 10% at the beginning of Dz1; it however decreases to *c.* 2% between 120.5 and 100.5 cm; but then subsequently increases to *c.* 15% at the end of Dz1 (Fig. 4b). The PD ratio is stable through Dz1 averaging 0.83.

4.4.2. Dz2, 95.5–55.5 cm (1047–621 cal yr BP), 7 samples

Zone Dz2 is characterised by gradually decreasing abundances of *B. spongium* from 62% to 38.6%. Conversely, Dz2 sees an increase in the abundance of both *I. paradoxum* (from *c. 0* to 12% at 95.5 cm) and *O. centrocarpum* (from *c.* 0.7%–8% between 95.5 cm and 81.5 cm; Fig. 4b). Additionally, the abundance of *Dubridinium* sp. increases at 74.5 cm from 0 to 6%. The PD ratio is high through Dz2 averaging at 1.59.

4.4.3. Dz3, 55.5–1.5 cm (621–3 cal yr BP), 19 samples

Zone Dz3 is dominated by a rapid large increase in the abundance of *Spiniferites ramosus* at 51.5 cm from 1 to 52%, and a gradual decrease in *Brigantedinium* and *B. spongium* (Fig. 4b). Many other dinocyst species also decrease notably throughout this zone, especially *O. centrocarpum, I. paradoxum* and *Dubridinium*. The PD ratio decreases and is stable through Dz3 averaging at 0.69.

4.4.4. Fossil dinocyst ordination

Dinocyst taxon scores were grouped on the DCA according to their modern day associated environmental parameters (Zonneveld et al., 2013). Taxon scores of species associated with fully marine environments and no river discharge (*I. paradoxum, Dubridinium* sp. and *Tuberculodinium vancampoae*) plot toward the positive on DCA axis 1 (Fig. 6a). Taxon scores of all other taxa characteristic of upwelling or which are cosmopolitan plot more negative on axis 1 (Fig. 6a). Sample scores from Dz2 plot in the bottom positive quadrat of the DCA ordination (Fig. 6b). Generally samples scores from Dz1 plot in the top positive quadrat of the DCA ordination. Sample scores from Dz3 plot mostly to the negative on DCA axis 1 (Fig. 6b).

5. Environmental reconstructions

Based on our age model (Fig. 2), we interpret pollen zones Pz2 and Pz3 (and dinocyst zones Dz2 and Dz3) identified within the OS73 core as most likely equivalent to the MCA and the LIA respectively. Additionally, the first two samples within PZ1 also fall within the Sassanid Period. Interestingly, the vegetation (and the grain-size) seems to respond quicker to the climate change than the dinocysts, with a *c.* 40 year delay in dinocyst assemblage changes at the beginning of the MCA and a lag of *c.* 240 years at the onset of the LIA (Fig. 4).

5.1. The sassanid period vegetation in S Iran and ocean dynamics in the Gulf of Oman

The overall dominance of Poaceae and low concentrations of Asteraceae suggests wet climatic conditions during the Sassanid period in S Iran (Fig. 4a; Fig. 7). A comparison of the abundance of the desert taxa Amaranthaceae during the three zones identified indicates that during the Sassanid period the climate was likely drier than during the LIA, but wetter than it was during the MCA. The DCA of sample scores supports this inference, with samples from Pz1 (during the Sassanid period), plotting more positive on DCA axis 1 (lower precipitation, more positive) than samples from the LIA, but more negative than samples from the MCA (Fig. 5b). In

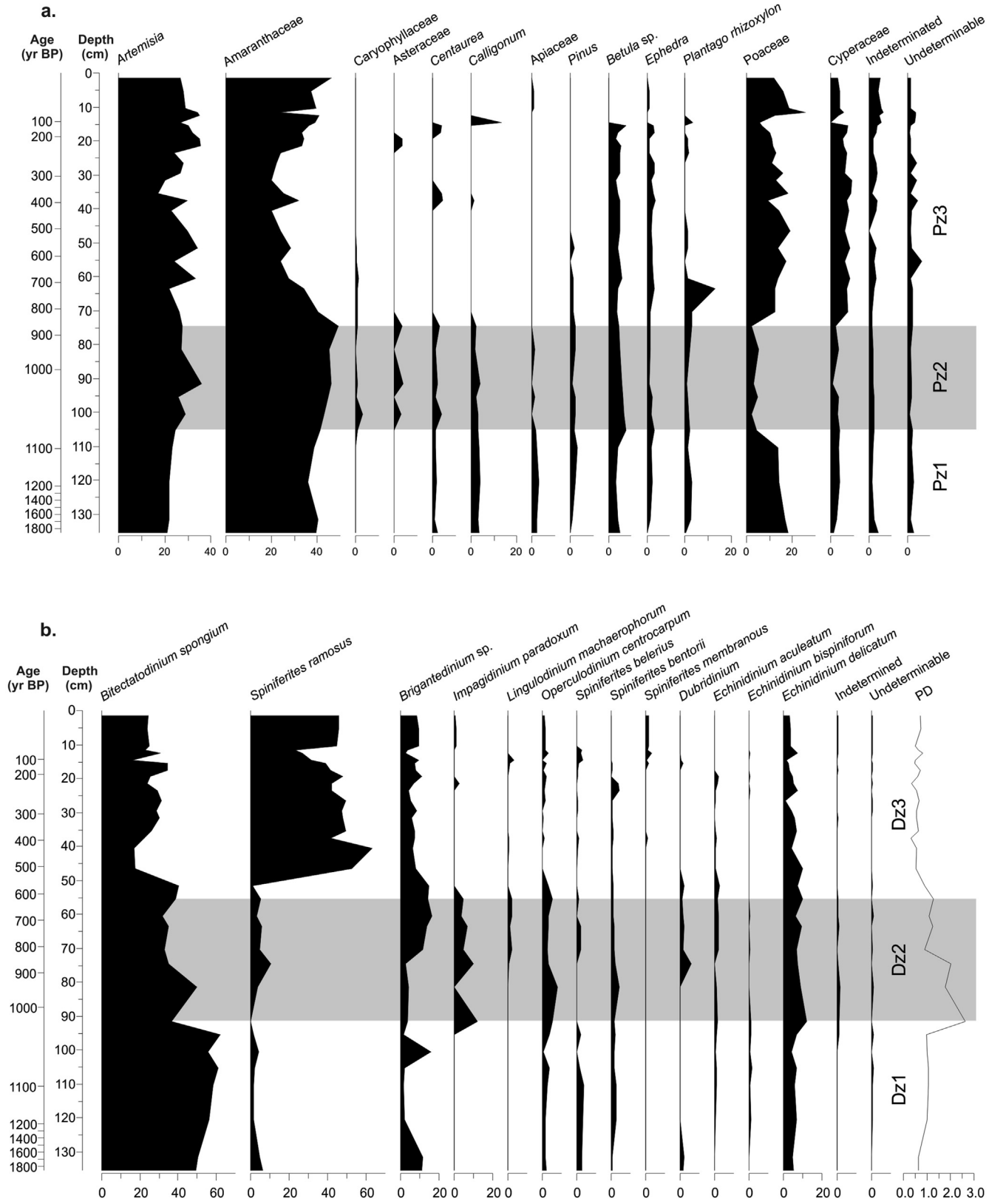

Fig. 4. a) Terrestrial pollen percentage diagram for core OS73 showing key taxa. b) Percentage dinocyst diagram for core OS73 showing key taxa. For the zonation method of the pollen and dinocyst diagrams see section 3.3. For full pollen and dinocyst diagram see Supplementary Figs. 1 and 2 respectively.

the marine realm, the abundance of *I. paradoxum* and *Dubridinium* sp. (species that dominate nutrient deficient environments) is low during the Sassanid period (Fig. 4b; Fig. 7), suggesting a high amount of freshwater discharge into the ocean. Increased moisture

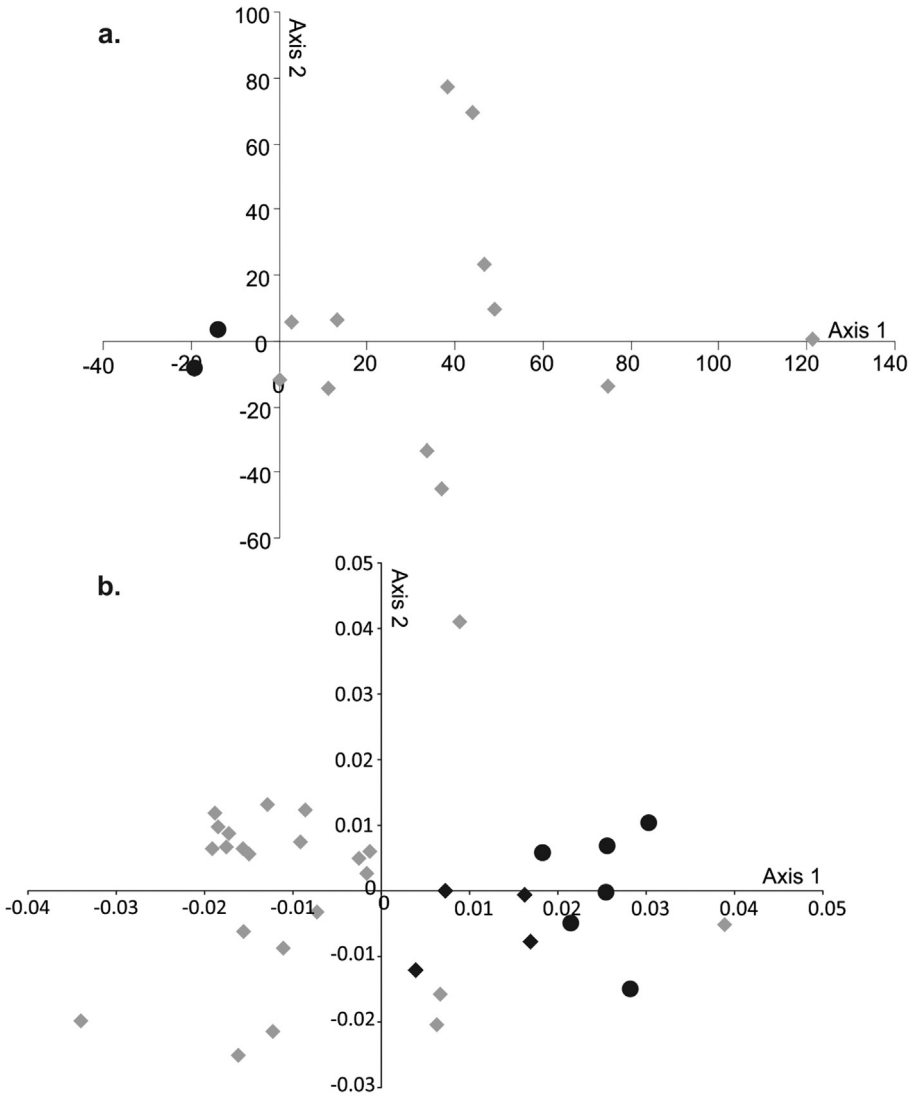

Fig. 5. Detrended correspondence analysis (DCA) pollen scores for core OS73. a) DCA taxon scores of all taxa representing >1% of the total pollen sum; black circles are taxa characteristic of wet climatic conditions, whilst grey diamonds represent taxa characteristic of dry climatic conditions. b) DCA sample scores; black circles are samples within Pz2 (dry climatic interval). Grey diamonds are samples within Pz3, and black diamonds are samples within Pz1 (representing wet climatic intervals).

availability is also evident at this time in Anatolia and in the Levant, and is thought to have facilitated settlement and agricultural expansion (Izdebski et al., 2016). The collapse of the Sassanid Empire at 651 CE is not evidenced by a change in climatic conditions in S Iran, with the end of the wet phase and the onset of dry conditions occurring later, at *c.* 925 CE (Fig. 7). Nevertheless increased dryness is already evidenced in Anatolia at *c.* 730 CE and in the Levant at *c.* 670 CE, and resulted in a change in the pattern of water use in the cities (Izdebski et al., 2016). Evidence from stalagmites indicates a series of severe droughts between 500 and 1000 CE in northern Oman (Fleitmann et al., 2009). Both our record and the record from Anatolia indicate that the decline in civilization seems to precede the early medieval drought. Although historical evidence points towards Arab invasion as a trigger to the collapse of organised large-scale cultivation, a combination of social changes and decreased precipitation would have certainly put additional stress on communities when water resources were already scarce, similar to what happened at that time around the Dead Sea (Leroy, 2010). Nevertheless, it should be noted that Anatolia and the Levant are more influenced by Mediterranean moisture bearing systems and thus have different hydroclimatic regimes to southern Iran.

5.2. Medieval climate anomaly vegetation in S Iran and ocean dynamics in the Gulf of Oman

The overall dominance of desert and semi-desert taxa such as Amaranthaceae, Asteraceae, *Artemisia, Calligonum* and *Centaurea* at the expense of grassland vegetation (Poaceae) suggests the environment throughout the MCA was exceptionally dry, even unable to support grassland vegetation (Fig. 4a; Fig. 7). At the onset of the MCA, a slight increase in clay abundance occurs (likely derived from windblown continental dust; Fig. 7h) and a rapid increase in sedimentation rate (Fig. 2), possibly caused by increased erosion from decreased vegetation cover during this time of extreme dryness, took place. Amaranthaceae dominates desert vegetation assemblages such as in the southern Iran Nubo-Sindian desert and semi-desert ecoregion, where annual precipitation is <100 mm yr^{-1} (Olson et al., 2001; Hooghiemstra et al., 2006). The presence of the fully open oceanic taxa *I. paradoxum* and *Dubridinium* sp (and lack of *S. ramosus;* Fig. 4b; Fig. 7) during the MCA, is

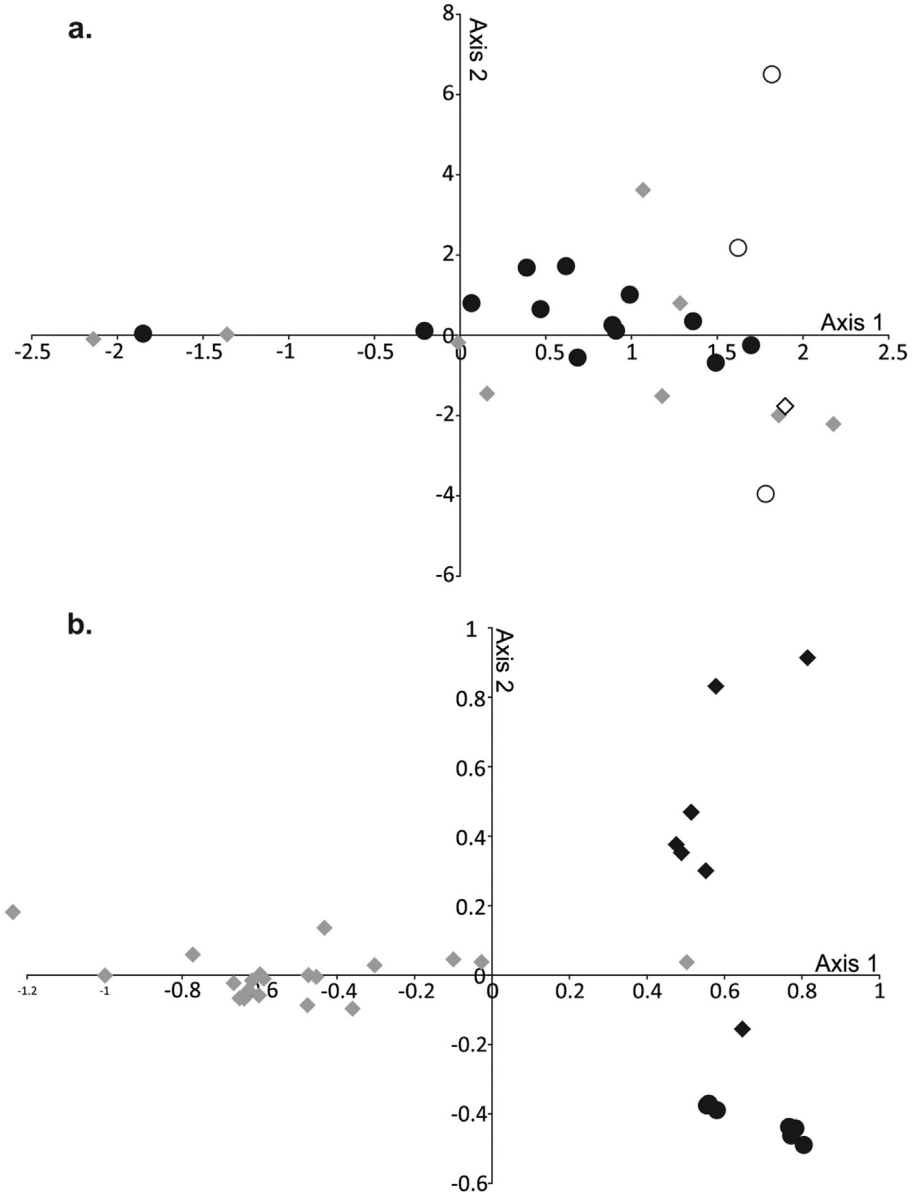

Fig. 6. Detrended correspondence analysis (DCA) dinocyst scores for core OS73. a) DCA taxon scores of all dinocysts representing >1% of the total dinocyst sum; black circles are taxa characteristic of coastal upwelling, grey diamonds represent cosmopolitan species, open circles are taxa representative of fully marine environments with no river discharge and open diamond is the taxon characteristic of upwelling conditions but no river discharge. b) DCA sample scores; black diamonds are samples within Dz1, black circles are samples within Dz2, and grey diamonds are samples within Dz3.

indicative of sea-surface salinities above 30, therefore suggesting little fluvial input into the ocean from the continent (Zonneveld et al., 2013). The high pollen to dinocyst ratio values indicate more terrestrial organic flux during the MCA (Fig. 4b), possibly due to: i) stronger winds (increased pollen transport), ii) increased local pollen production, or iii) lower concentrations of dinocysts. The increased abundance of clay during the MCA supports the hypothesis of stronger winds during the MCA. Additionally, with less river discharge and lower nutrient supply evidenced during the MCA, dinocyst populations would indeed reduce, resulting in the high PD values.

5.3. Little Ice Age vegetation in S Iran and ocean dynamics in the Gulf of Oman

The overall dominance of Poaceae, at the expense of Amaranthaceae and Asteraceae and the decrease in clay abundance throughout the LIA suggests a shift from desert to grassland vegetation, implying wetter conditions during the LIA in S Iran (Fig. 4a; Fig. 7). Modern ecoregions within close proximity to the coring locality where grass is a dominant component of the vegetation composition include the Zagros Mountain Forest Steppe and the Baluchistan Xeric Woodlands, where annual precipitation exceeds *c.* >150 mm yr^{-1}. Additionally, the abundance of *I. paradoxum* and *Dubridinium* sp. is low (Fig. 4b; Fig. 7), suggesting an increased amount of freshwater discharge into the ocean. The high abundance of *S. ramosus* (Fig. 7), a species particularly observed where the upper water salinity conditions are reduced permanently, again suggests more freshwater discharge into the ocean near the coring vicinity. The low pollen to dinocyst (PD) ratio values during the LIA (Fig. 4b) indicates more marine organic flux, likely due to increased nutrient supply promoting an increase in dinocyst populations.

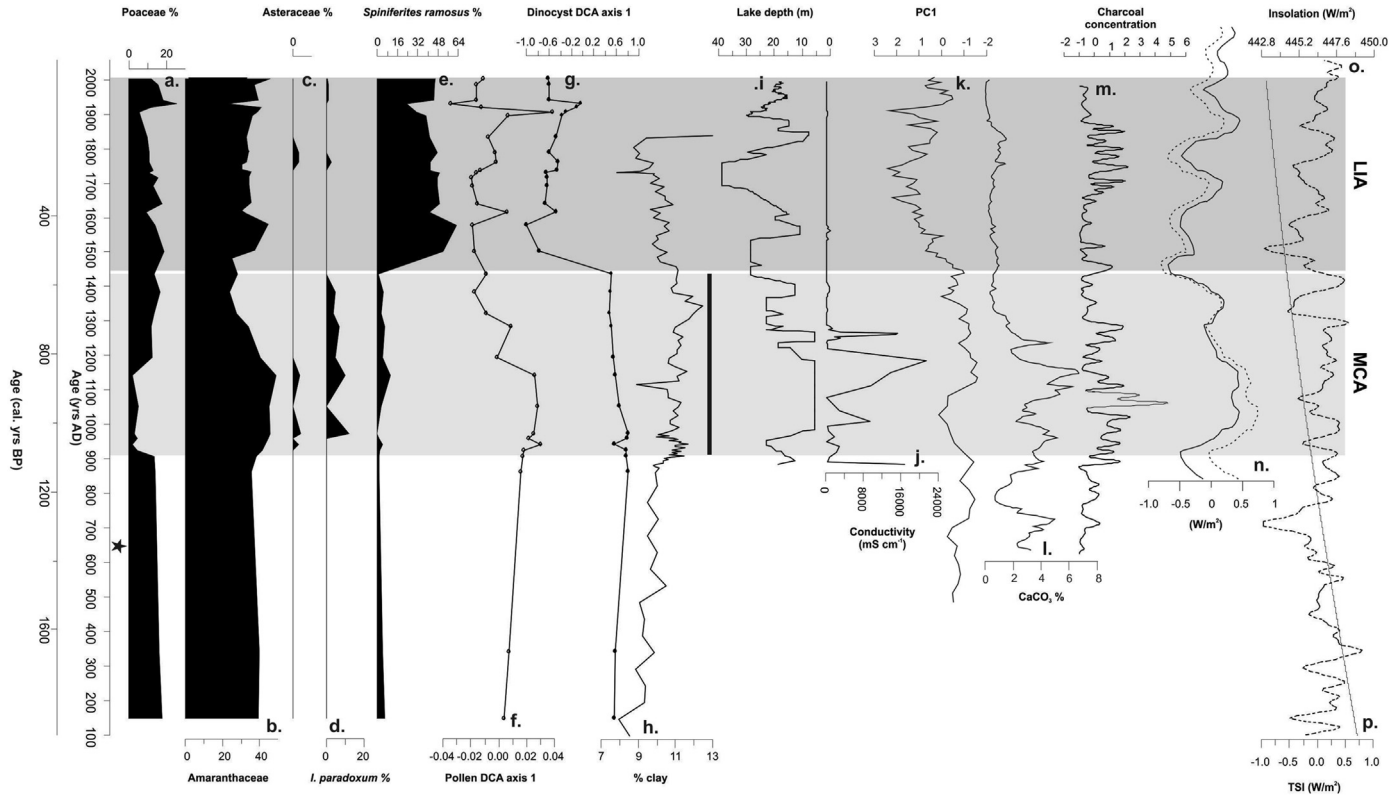

Fig. 7. a) OS73 Poaceae % (this study). b) OS73 Amaranthaceae % (this study). c) OS73 Asteraceae % (this study). d) OS73 *I. paradoxum* % (this study). e) OS73 *S. ramosus* % (this study). f) OS73 pollen DCA 1 axis (this study). g) OS73 dinocyst DCA 1 axis (this study). h) OS73 clay % (this study). Black bar highlights the period of high clay percentages. Note the axis is scaled, with 13% as a maximum cut-off value, and the value at 89.5 cm removed. i) Lake Naivasha diatom inferred depth (Verschuren et al., 2000). j) Lake Naivasha diatom inferred conductivity (Verschuren et al., 2000). k) Diatom PC1 axis from Tsuifong Lake, Taiwan (Wang et al., 2013). l) Lake Huguangyan $CaCO_3$% (Chu et al., 2002). m) Lake Tanganyika normalised charcoal (Tierney et al., 2010). n) Total solar forcing at 23.5°N (solid line), and total solar forcing at 23.5°S (dashed line), calculated by adding up the changes in solar output and orbital parameters (Yan et al., 2015). o) Mean insolation at 25° north (dashed line; Laskar et al., 2011). p) Global total solar irradiance (TSI; Steinhilber et al., 2009). All proxies (except *S. ramosus*) are plotted with 'right' indicating drier conditions. Grey shading is the combined pollen and dinocyst zonations for the Medieval Climate Anomaly (MCA) and the Little Ice Age (LIA). Black star indicates the collapse of the Sassanid Empire (651 AD).

5.4. The last 100 years of vegetation in S Iran and ocean dynamics in the Gulf of Oman

A decrease in *Betula* and a slight increase in Amaranthaceae abundance are evidenced during the last *c*. 100 years, which may indicate a slight reduction in moisture availability. *Betula* is found in the Pamir alpine desert and tundra ecoregion (Olson et al., 2001) in the Hindo Kush and the Himalayas and a decrease in *Betula* may imply a decrease in the strength of the Indian winter monsoonal winds and/or less river discharge into the Indian Ocean via Pakistan and India. This inference is supported by a corresponding increase in *I. paradoxum*, suggesting a reduction of freshwater discharge into the ocean. Our data support other studies that suggest that over the last century the Middle East has experienced severe drought, possibly as a result of anthropogenic global warming (IPCC, 2013). A shift to finer grain-sizes also indicates increased dryness and decreased vegetation cover from *c*. 1830 CE to present day.

6. Discussion

Although our data indicate wetter conditions during the LIA and drier conditions during the MCA, some other palaeoenvironmental data suggests, globally, that regions located around the northern limit of the ITCZ actually became drier during the LIA (relative to their climate during the MCA period) pointing to a possible southward shift of the ITCZ (Haug et al., 2001; Gupta et al., 2003; Fleitmann et al., 2004; Hodell et al., 2005; Yan et al., 2015). This southward shift of the ITCZ is the result of cool temperatures (caused by increased ice) in the northern hemisphere, inducing rapid cooling of the high and mid-latitudes. Subsequently wind-evaporation and SST feedbacks initiate the progression of a cold SST front towards ITCZ latitudes (Chiang and Bitz, 2005). When the cool SSTs reach the ITCZ, they cause it to shift southwards. Additionally, recent models suggest that more intense southern hemisphere summer insolation (relative to northern hemisphere summer insolation) results in the ITCZ migrating further south (Yan et al., 2015). Total solar forcing at approximately the latitude of OS73 (solid line; Fig 7n), and total solar forcing at 23.5°S (dashed line; Fig. 7n), calculated by adding up the changes in solar output and orbital parameters (Yan et al., 2015), indicate that the total amount of solar forcing in the southern hemisphere was indeed stronger during the LIA, providing further support that during the LIA the ITCZ likely migrated southwards.

Nevertheless the outcomes of our investigation clearly show that a southward migration of the ITCZ does not necessarily result in a change to a drier climatic regime in S Iran. In Iran, other proxy data also point to a generally wetter climate during the LIA and drier climate during the MCA. According to Kroonenberg et al. (2007) and Leroy et al. (2011), Caspian Sea level highstands coincide with periods of global cooling, with low sea level during the MCA and high during the LIA, due to increased precipitation, decreased evaporation and lower solar activity (Kroonenberg et al., 2007; Bard et al., 2011; Naderi Beni et al., 2013a). Moreover, globally, many other proxy records from similar tropical latitudes also

show a similar trend in increased moisture availability during the LIA, e.g Lake Chilwa in Malawi (Owen and Crossley, 1989), Lake Naivasha, Kenya (Verschuren et al., 2000), Lake Tanganyika (Tierney et al., 2010), Lake Huguangyan, China (Chu et al., 2002) and Tsuifong Lake, Taiwan (Wang et al., 2013, Fig. 7).

The southward migration of the ITCZ during times of cool northern hemisphere temperatures results in a displacement of northern hemisphere vegetation formations southward (Prentice and Jolly, 2000; Dupont, 2011; Miller and Gosling, 2014). A southward displacement of vegetation formations (and the associated precipitation regimes) in S Iran would likely result in the vegetation on the Makran coastline changing from desert and semi-desert to more steppe, grassland and woodland formations (Fig. 1; Olson et al., 2001). Additionally, to support the change in formations, precipitation must have increased, with rainfall likely similar to that to the north of the site today (Modarres and Rodrigues, 2007).

Conversely, the total amount of solar forcing in the northern hemisphere was stronger than in the southern hemisphere during the MCA (Fig. 7). This would have likely resulted in a northward migration of the ITCZ and an intensification of the Indian monsoonal system, resulting in an earlier spring maximum precipitation and a later autumn maximum precipitation along the Makran coastline (e.g. Shanahan et al., 2015). This shift in annual rainfall distribution would extend the length of the summer dry season, resulting in increased drought, causing an expansion of desert-type vegetation as evidenced in core OS73. The models of Rodwell and Hoskins (1996) also provide a 'monsoon-desert mechanism' where the intensification of the Indian monsoon (during times of maximum northern hemisphere summer insolation) leads to aridification in the Near East. Remote diabatic heating in the Asian monsoon region induces a Rossby-wave pattern to the west, resulting in adiabatic descent which is localised over the eastern Sahara and Mediterranean regions (Rodwell and Hoskins, 1996). Several studies in the eastern Sahara and Mediterranean indicate increased precipitation during northern hemisphere insolation minima (Kowalski, 1989; Djamali et al., 2010; Enzel et al., 2015). The monsoon-desert mechanism resulting in dry conditions in some regions of the Middle East associated with the northward shift of the ITCZ during the MCA may be similar to those causing the dry conditions which dominated the Early Holocene in the Near East (Djamali et al., 2010). Here it was proposed that a northward shift of the ITCZ caused the establishment of a high pressure system over NW Iran during the late spring, reducing the amount of spring rainfall and extending the length of the summer dry season (Djamali et al., 2010).

Although mangroves occur today in close proximity to the coring location (Spalding et al., 1997), and have been found in nearby sediment cores (102 km away in core OS55; Fig. 1; Miller et al., 2013) it is interesting to note the lack of any mangrove pollen taxa found in core OS73. It is likely that mangroves only existed in restricted pockets and never substantially expanded along the Makran coastline during the last 1900 years.

7. Conclusions

Fossil pollen and dinocyst data from marine core OS73 (Gulf of Oman) were used to reconstruct vegetation and ocean dynamics over the last 1900 years (AD >300). Both the pollen and dinocyst proxy records demonstrate three distinctive phases of vegetation succession in southern Iran and ocean dynamics in the Gulf of Oman. The OS73 record shows a period of savannah domination indicating relatively high precipitation from the base of the core at 150 CE until *c.* 910 CE, an interval which includes the Sassanid cultural period. The culmination of this wet period and subsequent replacement of savannah by desert formations may have increased environmental pressures on the already fragile societies after the Arab invasion at 651 CE. From *c.* 910 to 1145 CE, during the MCA, the vegetation was heavily dominated by desert formations, such as Amaranthaceae, Caryophyllaceae, Asteraceae, *Centaurea* and *Calligonum*. Additionally the presence of *I. paradoxum* and *Dubridinium* sp. indicate a drop in fluvial activity during this period. The desert taxa of the MCA were subsequently replaced by savannah formations at *c.* 1145 CE, comprised mainly of Poaceae and Cyperaceae, corresponding to the LIA, indicating a return to generally wetter climatic conditions. A sudden increase in *S. ramosus* at *c.* 1440 CE, during the LIA, suggests more freshwater discharge into the ocean near the coring vicinity.

With the northern hemispheric outpacing southern hemispheric global warming (Friedman et al., 2013), it is possible that the ITCZ will migrate northward (towards the warmer hemisphere). Our palaeoenvironmental proxy data supports current observations that a globally anthropogenically-induced warmer climate is likely to lead to increase drought severity in the Middle East.

Acknowledgements

CSM would like to thank L. Miller, G. Miller, Brunel University London and the Open University for financial support and the use of facilities. Gratitude is extended to S. Kershaw and C. Baeteman for pertinent discussions regarding interpretations.

Appendix A. Supplementary data

Supplementary data related to this article can be found at http://dx.doi.org/10.1016/j.quascirev.2016.05.010.

References

Abbaspour, K.C., Faramarzi, M., Ghasemi, S.S., Yang, H., 2009. Assessing the impact of climate change on water resources in Iran. Water Resour. Res. 45.
Ansari, M.H., Vink, A., 2007. Vegetation history and palaeoclimate of the past 30 kyr in Pakistan as inferred from the palynology of continental margin sediments off the Indus Delta. Rev. Palaeobot. Palynol. 145, 201–216.
Bard, E., Raisbeck, G., Yiou, F., Jouzel, J., 2011. Solar irradiance during the last 1200 years based on cosmogenic nuclides. Tellus B 52.
Bennett, K.D., 2003. Documentation for Psimpoll 4.10 and Pscomb 1.03: C Programs for Plotting Pollen Diagrams and Analysing Pollen Data. Quaternary Geology. University of Uppsala.
Blaauw, M., 2010. Methods and code for 'classical' age modelling of radiocarbon sequences. Quat. Geochronol. 5, 512–518.
Blott, S.J., Pye, K., 2001. GRADISTAT: a grain size distribution and statistics package for the analysis of unconsolidated sediments. Earth Surf. Process. Landf. 26, 1237–1248.
Bottema, S., 1986. A late quaternary pollen diagram from Lake Urmia (Northwestern Iran). Rev. Palaeobot. Palynol. 47, 241–261.
Bradley, R.S., Hughes, M.K., Diaz, H.F., 2003. Climate in medieval time. Science 302, 404–405.
Brock, J.C., McClain, C.R., Luther, M.E., Hay, W.W., 1991. The phytoplankton bloom in the northwest Arabian Sea during the southwest monsoon of 1979. J. Geophys. Res. 96, 20623–20642.
Burke, E.J., Brown, S.J., 2008. Evaluating uncertainties in the projection of future drought. J. Hydrometeorol. 9, 292–299.
Chiang, J.H., Bitz, C., 2005. Influence of high latitude ice cover on the marine Intertropical Convergence Zone. Clim. Dyn. 25, 477–496.
Chu, G., Liu, J., Sun, Q., Lu, H., Gu, Z., Wang, W., Liu, T., 2002. The 'mediaeval warm period' drought recorded in Lake Huguangyan, tropical south China. Holocene 12, 511–516.
Dai, A., 2013. Increasing drought under global warming in observations and models. Nat. Clim. Change 3, 52–58.
Danne-kar, A., 2005. Status of the Mangrove Forest of Iran. Workshop of Mangrove Ecology, Bandar Abbas.
de Vernal, A., 2009. Marine palynology and its use for studying nearshore environments. In: IOP Conference Series: Earth and Environmental Science, 5, p. 012002.
Dinpashoh, Y., Fakher-Fard, A., Moghaddam, M., Jahanbakhsh, S., Mirnia, M., 2004. Selection of variables for the purpose of regionalization of Iran's precipitation climate using multivariate methods. J. Hydrol. 297, 109–123.
Djamali, M., de Beaulieu, J.-L., Shah-hosseini, M., Andrieu-Ponel, V., Ponel, P.,

Amini, A., Akhani, H., Leroy, S.A.G., Stevens, L., Lahijani, H., Brewer, S., 2008. A late Pleistocene long pollen record from Lake Urmia, NW Iran. Quat. Res. 69, 413–420.
Djamali, M., de Beaulieu, J.-L., Andrieu-Ponel, V., Berberian, M., Miller, N.F., Gandouin, E., Lahijani, H., Shah-Hosseini, M., Ponel, P., Salimian, M., Guiter, F., 2009. A late Holocene pollen record from Lake Almalou in NW Iran: evidence for changing land-use in relation to some historical events during the last 3700 years. J. Archaeol. Sci. 36, 1364–1375.
Djamali, M., Akhani, H., Andrieu-Ponel, V., Braconnot, P., Brewer, S., de Beaulieu, J.-L., Fleitmann, D., Fleury, J., Gasse, F., Guibal, F., Jackson, S.T., Lézine, A.-M., Médail, F., Ponel, P., Roberts, N., Stevens, L., 2010. Indian Summer Monsoon variations could have affected the early-Holocene woodland expansion in the Near East. Holocene 20, 813–820.
Dupont, L., 2011. Orbital scale vegetation change in Africa. Quat. Sci. Rev. 30, 3589–3602.
El-Hames, A.S., Richards, K.S., 1998. An integrated, physically based model for arid region flash flood prediction capable of simulating dynamic transmission loss. J. Hydrol. Process. 12, 1219–1232.
Enzel, Y., Kushnir, Y., Quade, J., 2015. The middle Holocene climatic records from Arabia: reassessing lacustrine environments, shift of ITCZ in Arabian Sea, and impacts of the Southwest Indian and African monsoons. Glob. Planet. Change 129, 69–91.
Faegri, K., Iversen, J., 1989. Textbook of Pollen Analysis, fourth ed. Wiley, Chichester.
Fleitmann, D., Burns, S.J., Mudelsee, M., Neff, U., Kramers, J., Mangini, A., Matter, A., 2003. Holocene forcing of the Indian monsoon recorded in a stalagmite from Southern Oman. Science 300, 1737–1739.
Fleitmann, D., Burns, S.J., Neff, U., Mudelsee, M., Mangini, A., Matter, A., 2004. Palaeoclimatic interpretation of high-resolution oxygen isotope profiles derived from annually laminated speleothems from Southern Oman. Quat. Sci. Rev. 23, 935–945.
Fleitmann, D., Mudelsee, M., Bradley, R.S., Pickering, P., Kramers, J., Burns, S.J., Mangini, A., Matter, A., 2009. Megadroughts at the dawn of Islam recorded in a 2600-year long stalagmite from Northern Oman. Geophys. Res. Abstr. 11. EGU2009-8174-1.
Folk, R.L., Ward, W.C., 1957. Brazos River bar: a study in the significance of grain size parameters. J. Sediment. Petrol. 27, 3–26.
Friedman, A.R., Hwang, Y.-T., Chiang, J.C.H., Frierson, D.M.W., 2013. Interhemispheric temperature asymmetry over the twentieth century and in future projections. J. Clim. 26, 5419–5433.
Gosling, W.D., Miller, C.S., Livingstone, D.A., 2013. Atlas of the tropical West African pollen flora. Rev. Palaeobot. Palynol. 199, 1–135.
Graham, N.E., Ammann, C.M., Fleitmann, D., Cobb, K.M., Luterbacher, J., 2011. Support for global climate reorganization during the "medieval climate anomaly". Clim. Dyn. 37, 1217–1245.
Guiot, J., 2012. A robust spatial reconstruction of April to September temperature in Europe: comparisons between the medieval period and the recent warming with a focus on extreme values. Glob. Planet. Change 84–85, 14–22.
Gupta, A.K., Anderson, D.M., Overpeck, J.T., 2003. Abrupt changes in the Asian southwest monsoon during the holocene and their links to the North Atlantic Ocean. Nature 421, 354–357.
Haghani, S., Leroy, S.A.G., Khdir, S., Kabiri, K., Naderi Beni, M., Lahijani, H.A.K., 2015. An early Little Ice Age brackish water invasion along the coast of the Caspian Sea (sediment of Langarud wetland) and its wider impacts on the environment and people. Holocene Online 26 (1), 3–16.
Hartmann, D.L., Klein Tank, A.M.G., Rusticucci, M., Alexander, L.V., Brönnimann, S., Charabi, Y., Dentener, F.J., Dlugokencky, E.J., Easterling, D.R., Kaplan, A., Soden, B.J., Thorne, P.W., Wild, M., Zhai, P.M., 2013. Observations: Atmosphere and Surface. Cambridge University Press, Cambridge.
Haug, G.H., Hughen, K.A., Sigman, D.M., Peterson, L.C., Rohl, U., 2001. Southward migration of the intertropical convergence zone through the holocene. Science 293, 1304–1308.
Hodell, D.A., Brenner, M., Curtis, J.H., Medina-González, R., Ildefonso-Chan Can, E., Albornaz-Pat, A., Guilderson, T.P., 2005. Climate change on the Yucatan Peninsula during the Little Ice Age. Quat. Res. 63, 109–121.
Hooghiemstra, H., Lézine, A.-M., Leroy, S.A.G., Dupont, L., Marret, F., 2006. Late Quaternary palynology in marine sediments: a synthesis of the understanding of pollen distribution patterns in the NW African setting. Quat. Int. 148, 29–44.
IPCC, 2007. Climate Change 2007: The Physical Science Basis. Contribution of Working Group I to the Fourth Assessment Report of the Intergovernmental Panel on Climate Change. Cambridge Univiersity Press, Cambridge & New York.
IPCC, 2013. Climate change 2013: the physical science basis. Contribution of Working Group I of the Fifth Assessment Report of the Intergovernmental Panel on Climate Change. Cambridge Univiersity Press, Cambridge & New York.
Ivory, S.J., Lézine, A.-M., 2009. Climate and environmental change at the end of the Holocene Humid Period: a pollen record off Pakistan. Comptes Rendus Geosci. 341, 760–769.
Izdebski, A., Pickett, J., Roberts, N., Waliszewski, T., 2016. The environmental, archaeological and historical evidence for regional climatic changes and their societal impacts in the Eastern Mediterranean in Late Antiquity. Quat. Sci. Rev. 136, 189–208.
Jones, P.D., Mann, M.E., 2004. Climate over past millennia. Rev. Geophys. 42.
Juggins, S., 2005. C2 Program Version 1.5. Department of Geography. University of Newcastle, Newcastle upon Tyne, UK.
Kowalski, K., Neer, W.v., Bocheński, Z., Młynarski, M., Rzebik-Kowalska, B., Szyndlar, Z., Gautier, A., Schild, R., Close, A.E., Wendorf, F., 1989. A last interglacial fauna from the Eastern Sahara. Quat. Res. 32, 335–341.
Kroonenberg, S.B., Abdurakhmanov, G.M., Badyukova, E.N., van der Borg, K., Kalashnikov, A., Kasimov, N.S., Rychagov, G.I., Svitoch, A.A., Vonhof, H.B., Wesselingh, F.P., 2007. Solar-forced 2600 BP and Little Ice Age highstands of the Caspian sea. Quat. Int. 173–174, 137–143.
Lamb, H., 1977. Climatic History and the Future. Methuen and Co. Ltd., London, England.
Laskar, J., Fienga, A., Gastineau, M., Manche, H., 2011. La2010: a new orbital solution for the long-term motion. Astron. Astrophys. 532.
Leroy, S.A.G., 2010. Pollen analysis of core DS7-1 (Dead Sea) showing intertwined effects of climatic change and human activities in the Late Holocene. J. Archaeol. Sci. 37, 306–316.
Leroy, S.A.G., Marret, F., Gibert, E., Chalie, F., Reyss, J.L., Arpe, K., 2007. River inflow and salinity changes in the Caspian Sea during the last 5500 years. Quat. Sci. Rev. 26, 3359–3383.
Leroy, S.A.G., Lahijani, H.A.K., Djamali, M., Naqinezhad, A., Moghadam, M.V., Arpe, K., Shah-Hosseini, M., Hosseindoust, M., Miller, C.S., Tavakoli, V., Habibi, P., Naderi Beni, M., 2011. Late Little Ice Age palaeoenvironmental records from the anzali and amirkola lagoons (South caspian sea): vegetation and sea level changes. Palaeogeogr. Palaeoclimatol. Palaeoecol. 302, 415–434.
Leroy, S.A.G., Kakroodi, A.A., Kroonenberg, S., Lahijani, H.K., Alimohammadian, H., Nigarov, A., 2013a. Holocene vegetation history and sea level changes in the SE corner of the caspian sea: relevance to SW Asia climate. Quat. Sci. Rev. 70, 28–47.
Leroy, S.A.G., Tudryn, A., Chalié, F., López-Merino, L., Gasse, F., 2013b. From the Allerød to the mid-Holocene: palynological evidence from the south basin of the Caspian Sea. Quat. Sci. Rev. 78, 77–97.
Leroy, S.A.G., López-Merino, L., Tudryn, A., Chalié, F., Gasse, F., 2014. Late Pleistocene and Holocene palaeoenvironments in and around the middle Caspian basin as reconstructed from a deep-sea core. Quat. Sci. Rev. 101, 91–110.
Lézine, A.M., 2005. African Pollen Database. http://medias.obs-mip.fr/apd/accueil.htm.
Lézine, A.-M., 2009. Timing of vegetation changes at the end of the Holocene Humid Period in desert areas at the northern edge of the Atlantic and Indian monsoon systems. Comptes Rendus Geosci. 341, 750–759.
Lézine, A.-M., Tiercelin, J.J., Robert, C., Saliège, J.-F., Cleuziou, S., Inizan, M.-L., Braemer, F., 2007. Centennial to millennial-scale variability of the Indian monsoon during the early Holocene from a sediment, pollen and isotope record from the desert of Yemen. Palaeogeogr. Palaeoclimatol. Palaeoecol. 243, 235–249.
McCarthy, F.M.G., Mudie, P.J., 1998. Oceanic pollen transport and pollen:dinocyst ratios as markers of late Cenozoic sea level change and sediment transport. Palaeogeogr. Palaeoclimatol. Palaeoecol. 138, 187–206.
Meher-Homji, V.M., 1971. On the mediterranean climatic regime of West Pakistan. Arch. für Meteorol. Geophys. Bioklimatol. Ser. B 19, 277–286.
Milani, A.S., Lak, R., Beiglu, M.J., 2013. Monitoring the area and distribution of mangrove forests in the southern coasts of Iran. J. Environ. Treat. Tech. 1, 137–146.
Miller, C.S., Gosling, W.D., 2014. Quaternary forest associations in lowland tropical West Africa. Quat. Sci. Rev. 84, 7–25.
Miller, C.S., Leroy, S.A.G., Izon, G., Lahijani, H.A.K., Marret, F., Cundy, A.B., Teasdale, P.A., 2013. Palynology: a tool to identify abrupt events? an example from Chabahan Bay, southern Iran. Mar. Geol. 337, 195–201.
Min, S.-K., Zhang, X., Zwiers, F.W., Hegerl, G.C., 2011. Human contribution to more-intense precipitation extremes. Nature 470, 378–381.
Modarres, R., Rodrigues, V.P., 2007. Rainfall trends in arid and semi-arid regions of Iran. J. Arid Environ. 70, 344–355.
Molavi-Arabshahi, M., Arpe, K., Leroy, S.A.G., 2015. Precipitation and temperature of the Southwest Caspian Sea during the last 56 years, their trends and teleconnections with large-scale atmospheric phenomena. Int. J. Climatol. 36, 2156–2172. http://dx.doi.org/10.1002/joc.4483.
Moradi, Y., Said, M., Abustan, I., 2011. Drought impacts and vulnerability in Isfahan province. World academy of science. Eng. Technol. 5.
Motagh, M., Walter, T.R., Sharifi, M.A., Fielding, E., Schenk, A., Anderssohn, J., Zschau, J., 2008. Land subsidence in Iran caused by widespread water reservoir overexploitation. Geophys. Res. Lett. 35, L16403.
Naderi Beni, A., Lahijani, H., Mousavi Harami, R., Arpe, K., Leroy, S.A.G., Marriner, N., Berberian, M., Ponel, V.A., Djamali, M., Mahboubi, A., Reimer, P.J., 2013a. Caspian sea level changes during the last millennium: historical and geological evidences from the south Caspian Sea. Clim. Past 9, 1645–1665.
Naderi Beni, A., Lahijani, H., Moussavi Harami, R., Leroy, S.A.G., Shah-Hosseini, M., Kabiri, K., Tavakoli, V., 2013b. Development of spit–lagoon complexes in response to Little Ice Age rapid sea-level changes in the central Guilan coast, South Caspian Sea, Iran. Geomorphology 187, 11–26.
New, M., Hulme, M., Jones, P.D., 2000. Representing twentieth century space time climate variability. Part 2: development of 1901-96 monthly grids of terrestrial surface climate. J. Clim. 13, 2217–2238.
Olson, D.M., Dinerstein, E., Wikramanayake, E.D., Burgess, N.D., Powell, G.V.N., Underwood, E.C., D'Amico, J.A., Itoua, I., Strand, H.E., Morrison, J.C., Louks, C.J., Allnutt, T.F., Ricketts, T.H., Kura, Y., Lamoreux, J.F., Wettengel, W.W., Hedao, P., Kassem, K.R., 2001. Terrestrial ecoregions of the world: a new map of life on earth. BioScience 51, 933–938.
Omrani, R.H., Sauer, E., Wilkinson, T., Safari Tamak, E., Ainslie, R., Mahmoudi, M., Griffiths, S., Ershadi, M., Jansen Van Rensburg, J., Fattahi, M., Ratcliffe, J., Nokandeh, J., Nazifi, A., Thomas, R., Gale, R., Hoffmann, B., Sauer, E., Omrani

Rekavadi, H., Wilkinson, T., Safari Tamak, E., Ainslie, R., Mahmoudi, M., Griffiths, S., Ershadi, M., Jansen Van Rensburg, J., Fattahi, M., Ratcliffe, J., Nokandeh, J., Nazifi, A., Thomas, R., Gale, R., Hoffmann, B., 2007. An imperial frontier of the Sasanian Empire: further fieldwork at the Great Wall of Gorgan, Iran. J. Br. Inst. Persian Stud. 45, 95–136.
Overpeck, J., Anderson, D., Trumbore, S., Prell, W., 1996. The SW Indian Monsoon over the last 18,000 years. Clim. Dyn. 12, 213–225.
Owen, R.B., Crossley, R., 1989. Recent sedimentation in lakes Chilwa and Chiuta, Malawi. Palaeoecol. Afr. 20, 109–117.
Parker, A.G., Eckersley, L., Smith, M.M., Goudie, A.S., Stokes, S., Ward, S., White, K., Hodson, M.J., 2004. Holocene vegetation dynamics in the northeastern Rub' al-Khali desert, Arabian Peninsula: a phytolith, pollen and carbon isotope study. J. Quat. Sci. 19, 665–676.
Prell, W.L., Campo, E.V., 1986. Coherent response of Arabian Sea upwelling and pollen transport to late Quaternary monsoonal winds. Nature 323, 526–528.
Prentice, I.C., Jolly, D., 2000. BIOME 6000 participants., Mid-Holocene and glacial-maximum vegetation geography of the northern continents and Africa. J. Biogeogr. 27, 507–519.
Qasim, S.Z., 1982. Oceanography of the northern Arabian sea. Deep Sea Res. 29, 1041–1068.
Reille, M., 1995. Pollen et spores d'Europe et d'Afrique du Nord. Laboratoire de Botanique Historique et Palynologie.
Rind, D., Goldberg, R., Hansen, J., Rosenzweig, C., Ruedy, R., 1990. Potential evapotranspiration and the likelihood of future drought. J. Geophys. Res. 95, 9983–10004.
Rochon, A., Vernal, A.D., Turon, J.L., Matthießen, J., Head, M.J., 1999. Distribution of recent dinoflagellate cysts in surface sediments from the North Atlantic Ocean and adjacent seas in relation to sea-surface parameters. Am. Assoc. Stratigr. Palynol. Contrib. Ser. 35, 1–146.
Rodwell, M.J., Hoskins, B.J., 1996. Monsoons and the dynamics of deserts. Q.J.R. Meteorol. Soc. 122, 1385–1404.
Rosenthal, Y., Linsley, B.K., Oppo, D.W., 2013. Pacific ocean heat content during the past 10,000 years. Science 342, 617–621.
Schott, F., Swallow, J.C., Fieux, M., 1996. The Somali current at the equator: annual cycle of currents and transports in the upper 1000m and connection to neighbouring latitudes. Deep Sea Res. 37, 1825–1848.
Seager, R., Ting, M., Held, I., Kushnir, Y., Lu, J., Vecchi, G., Huang, H.-P., Harnik, N., Leetmaa, A., Lau, N.-C., Li, C., Velez, J., Naik, N., 2007. Model projections of an imminent transition to a more arid climate in Southwestern North America. Science 316, 1181–1184.
Shanahan, T.M., McKay, N.P., Hughen, K.A., Overpeck, J.T., Otto-Bliesner, B., Heil, C.W., King, J., Scholz, C.A., Peck, J., 2015. The time-transgressive termination of the African humid period. Nat. Geosci. 8, 140–144.
Sharifi, A., Pourmand, A., Canuel, E.A., Ferer-Tyler, E., Peterson, L.C., Aichner, B., Feakins, S.J., Daryaee, T., Djamali, M., Beni, A.N., Lahijani, H.A.K., Swart, P.K., 2015. Abrupt climate variability since the last deglaciation based on a high-resolution, multi-proxy peat record from NW Iran: the hand that rocked the Cradle of Civilization? Quat. Sci. Rev. 123, 215–230.
Sheffield, J., Wood, E., 2008. Projected changes in drought occurrence under future global warming from multi-model, multi-scenario, IPCC AR4 simulations. Clim. Dyn. 31, 79–105.
Smith, S.L., Banse, K., Cochran, J.K., Codispoti, L.A., Ducklow, H.W., Luther, M.E., Olson, D.B., Peterson, W.T., Prell, W.L., Surgi, N., Swallow, J.C., Wishner, K., 1991. U.S. JGOFS: Arabian Sea Process Study US JGOFS Planning Report Woods Hole: WHOI, p. 164.
Snead, R.E., 1968. Weather patterns in Southern West Pakistan. Arch. für Meteorol. Geophys. Bioklimatol. Ser. B 16, 316–346.
Spalding, M., Blasco, F., Field, C., 1997. World Mangrove Atlas. International Society for Mangrove Ecosystems.
Steinhilber, F., Beer, J., Fröhlich, C., 2009. Total solar irradiance during the Holocene. Geophys. Res. Lett. 36.
Stockmarr, J., 1972. Tablets with spores used in absolute pollen analysis. Pollen Spore XIII, 615–621.
Stuiver, M., Reimer, P.J., 2005. CALIB 5.0. Program and Documentation.
Tierney, J.E., Mayes, M.T., Meyer, N., Johnson, C., Swarzenski, P.W., Cohen, A.S., Russell, J.M., 2010. Late-twentieth-century warming in Lake Tanganyika unprecedented since AD 500. Nat. Geosci. 3, 422–425.
Van Zeist, W., Bottema, S., 1977. Palynological investigations in Western Iran. Palaeohistoria 19, 19–85.
Verschuren, D., Laird, K.R., Cumming, B.F., 2000. Rainfall and drought in equatorial east Africa during the past 1,100 years. Nature 403, 410–414.
Wang, G., 2005. Agricultural drought in a future climate: results from 15 global climate models participating in the IPCC 4th assessment. Clim. Dyn. 25, 739–753.
Wang, L.-C., Behling, H., Lee, T.-Q., Li, H.-C., Huh, C.-A., Shiau, L.-J., Chen, S.-H., Wu, J.-T., 2013. Increased precipitation during the Little Ice Age in northern Taiwan inferred from diatoms and geochemistry in a sediment core from a subalpine lake. J. Paleolimnol. 49, 619–631.
Wyrtki, K., 1973. Physical oceanography of the Indian Ocean. In: Zeitzschel, B., Gerlach, S.A. (Eds.), The Biology of the Indian Ocean. Springer, Berlin, pp. 18–36.
Yan, H., Wei, W., Soon, W., An, Z., Zhou, W., Liu, Z., Wang, Y., Carter, R.M., 2015. Dynamics of the intertropical convergence zone over the western Pacific during the Little Ice Age. Nat. Geosci. 8, 315–320.
Zohary, M., 1973. Geobotanical Foundations of the Middle East. Gustav Fischer Verlag, Stuttgart, Germany.
Zonneveld, K.A.F., Jurkschat, T., 1999. Bitectatodinium spongium (Zonneveld, 1997) Zonneveld et Jurkschat, comb. nov. from modern sediments and sediment trap samples of the Arabian Sea (northwestern Indian Ocean): taxonomy and ecological affinity. Rev. Palaeobot. Palynol. 106, 153–169.
Zonneveld, K.A.F., Versteegh, G.J.M., de Lange, G.J., 1997. Preservation of organic-walled dinoflagellate cysts in different oxygen regimes: a 10,000 year natural experiment. Mar. Micropaleontol. 29, 393–405.
Zonneveld, K., Marret, F., Versteegh, G., Bogusa, K., Bonnet, S., Bouimetarhanan, I., Crouche, E., Vernald, A., Elshanawanya, R., Edwards, L., Esper, O., Forke, S., Grøsfjeld, K., Henry, M., Holzwarth, U., Kielt, J., Kim, S., Ladouceur, S., Ledu, D., Chen, L., Limoges, A., Londeix, L., Lu, S.H., Mahmoud, M., Marinol, G., Matsouka, K., Matthiessen, J., Mildenhal, D.C., Mudie, P., Neil, H.L., Pospelova, V., Qi, Y., Radi, T., Richerol, T., Rochon, A., Sangiorgi, F., Solignac, S., Turon, J.L., Verleye, T., Wang, Y., Wang, Z., Young, M., 2013. Atlas of modern dinoflagellate cyst distribution based on 2405 data points. Rev. Palaeobot. Palynol. 191, 1–197.